LAWRENCE
LIVERMORE
NATIONAL
LABORATORY

UCRL-JRNL-236328

Relativistic many-body calculations of lifetimes, rates, and line strengths of multipole transitions between 3l-1 4l' states in Ni-like ions

U. I. Safronova, A. S. Safronova, P. Beiersdorfer

November 7, 2007

Physical Review A

Disclaimer

Relativistic many-body calculations of lifetimes, rates, and line strengths of multipole transitions between $3l^{-1}4l'$ states in Ni-like ions

U. I. Safronova, A. S. Safronova
Physics Department, University of Nevada, Reno, NV 89557, USA

P. Beiersdorfer
Lawrence Livermore National Laboratory, Livermore, CA 94550, USA

Transition rates and line strengths are calculated for electric-multipole (E2 and E3) and magnetic-multipole (M1, M2, and M3) transitions between $3s^23p^63d^{10}$, $3s^23p^63d^94l$, $3s^23p^53d^{10}4l$, and $3s3p^63d^{10}4l$ states (with $4l = 4s$, $4p$, $4d$, and $4f$) in Ni-like ions with the nuclear charges ranging from $Z = 34$ to 100. Relativistic many-body perturbation theory (RMBPT), including the Breit interaction, is used to evaluate retarded multipole matrix elements. Transition energies used in the calculation of line strengths and transition rates are from second-order RMBPT. Lifetimes of the $3s^23p^63d^94s$ levels are given for $Z = 34$–100. Taking into account that calculations were performed in a very broad range of Z, most of the data are presented in graphs as Z-dependencies. The full set of data is given only for Ni-like W ion. In addition, we also give complete results for the $3d4s\ ^3D_2 - 3d4s\ ^3D_1$ magnetic-dipole transition, as the transition may be observed in future experiments, which measure both transition energies and radiative rates. These atomic data are important in the modeling of radiation spectra from Ni-like multiply-charged ions generated in electron beam ion trap experiments as well as for laboratory plasma diagnostics including fusion research.

I. INTRODUCTION

Recently, the observation and wavelength measurements of magnetic-dipole (M1), electric-quadrupole (E2), and magnetic-octupole (M3) decays of long-lived levels in Ni-like ions Xe^{26+}, Cs^{27+}, and Ba^{28+} was reported by Träbert *et al.* [1]. The lifetime of the lowest $3d^94s\ ^3D_3$ level was determined by using time-resolved soft-x-ray spectroscopy on the Livermore EBIT-I electron beam ion trap. An analysis of the metastable levels in nickellike ions was also presented by Träbert *et al.* [2]. The M3 line in Xe^{26+} was observed using the Livermore EBIT-I electron beam ion trap and a microcalorimeter, as well as a high-resolution flat-field grating spectrometer. It was underlined in [2] that long-lived excited levels are of interest for the detailed understanding of atomic structure and high-multipole order decay processes. An observation of a blend of E2 and M3 lines in Ni-like tungsten spectra obtained from tungsten ions produced by electron impact in the electron beam ion trap (EBIT) operating at the National Institute of Standards and Technology (NIST) was recently presented by Ralchenko *et al.* [3]. These observations follow the first spectrally resolved identification of E2 and M3 decay in the x-ray spectrum of Ni-like Th^{62+} and U^{64+} reported by Beiersdorfer *et al.* [4] more than fifteen years ago.

The relative magnitudes of the electric-multipole (E1, E2, and E3) and magnetic-multipole (M1, M2, and M3) radiative decay rates calculated by the MCDF approach were presented by Biémont [5] for the lowest 17 levels of highly ionized nickel-like ions. The importance of the octupole decays in atomic spectra was also pointed out in [6]. Recently, Yao *et al.* [7, 8] presented extensive multiconfiguration Dirac-Fock calculations that showed the hyperfine quenching of the magnetic octupole decay of $3d^94s\ ^3D_3$ and state mixing between the $^3D_3$ and $^3D_2$ levels due to hyperfine interaction in the Xe^{26+} ion. Subsequently, observation of hyperfine mixing in measurements of the magnetic octupole decay in isotopically pure nickel-like ^{129}Xe and ^{132}Xe ions was reported by Träbert *et al.* [9].

Calculated values of transition wavelengths and rates for Ni-like ions with $36 \leq Z \leq 100$ presented by Hamasha *et al.* in Ref. [10] were obtained by using the relativistic many-body perturbation theory (RMBPT) method. In particular, reduced matrix elements, line strengths, and transition rates to the ground state for all possible electric- and magnetic-dipole and electric- and magnetic-quadrupole transitions (E1, M1, E2, M2) in Ni-like ions were given in [10]. Relativistic many-body calculations of multipole (E1, M1, E2, M2, E3, M3) transition wavelengths and rates between $3l^{-1}4l'$ excited and ground states in nickel-like ions were reported by Safronova *et al.* in Ref. [11]. Multipole (E1, M1, E2, M2, E3, M3) transition wavelengths and rates between $3l^{-1}5l'$ excited and ground states in nickel-like ions were recently presented [12].

In the present paper, RMBPT is used to determine matrix elements, line strengths, and transition rates for electric multipole (E2 and E3) and magnetic multipole (M1, M2, and M3) transitions between $3s^23p^63d^{10}$, $3s^23p^63d^94l$, $3s^23p^53d^{10}4l$, and $3s3p^63d^{10}4l$ excited states (with $4l = 4s$, $4p$, $4d$, and $4f$) in Ni-like ions with the nuclear charges ranging from $Z = 34$ to 100. Calculations are carried out to second order in perturbation theory. Lifetimes of the $3s^23p^63d^94s$ levels are given for $Z = 34$–100. Taking into account that calculations were performed in a very broad range of Z, most of the data are presented in graphs as Z-dependencies. However, a detailed discussion of the various contributions to the dipole matrix elements and energy levels is

given for nickellike tungsten ($Z = 74$). The relativistic atomic data for this particular ion is important for the study of the variety of laboratory plasmas such as for tokamaks [13, 14], x-ray lasers [15], z-pinches [16–18]. Also and radiation from Ni-like W has been studied in electron beam ion traps [17, 19–21].

In the next section, we briefly review the RMBPT theory for multipole transition matrix elements. Examples of E2, E3, M1, M2, and M3 matrix elements are given in Tables I and II for W^{46+}. E2 and E3 coupled reduced matrix elements calculated in length L and velocity V forms are compared in Table III for W^{46+}. Line strengths for M1, M2, and M3 transitions in Ni-like ions are presented as a function of Z in Fig. 1. E2, E3, M1, M2, and M3 transition rates are discussed in Sec. III. Transition rates for E2, E3, M1, M2, and M3 transition and lifetimes of the $3d^9 4s\ ^{1,3}D_J$ states in Ni-like ions are illustrated graphically in Fig. 2 and 3. RMBPT energies and radiative rates for M1 and E2 transitions are compared with MCDF results [5] in Table V.

II. MULTIPOLE MATRIX ELEMENTS BETWEEN EXCITED HOLE-PARTICLE STATES

The first-order reduced K-pole matrix element $Z_K^{(1)}$ for transitions between hole-particle states $av(J)$ and $cw(J')$ is given by

$$\begin{aligned} & Z_K^{(1)}(av(J), cw(J')) \\ = \; & \sqrt{[J][J']}(-1)^{K+j_v+j_c} \\ & \times \left[\delta(c,a) Z_K(wv)(-1)^{J'} \begin{Bmatrix} J & J' & K \\ j_w & j_v & j_a \end{Bmatrix} \right. \\ & \left. +\delta(w,v) Z_K(ca)(-1)^{J} \begin{Bmatrix} J & J' & K \\ j_c & j_a & j_v \end{Bmatrix}\right], \end{aligned} \tag{1}$$

where $[J] = 2J+1$. The K-pole matrix elements $Z_K(wv)$ and $Z_K(ca)$, which include retardation, are given by Eqs. (38,39) of Ref. [22] and Appendix A of Ref. [10].

The second-order reduced matrix element $Z_K^{(2)}$ for the transition between the hole-particle states $av(J)$–$cw(J')$ consists of four contributions: Dirac-Fock (DF) term ($Z_K^{(\mathrm{DF})}$), random-phase approximation (RPA) term ($Z_K^{(\mathrm{RPA})}$), correlation contribution ($Z_K^{(\mathrm{RPA})}$), and derivative term, $Z_K^{(\mathrm{derv})}$:

$$\begin{aligned} & Z_K^{(\mathrm{DF})}(av(J), cw(J')) = \sqrt{[J][J']}(-1)^{K+j_c+j_v} \\ & \times \sum_n \left[\delta(ca) \left(\frac{Z_K(wn)\Delta(nv)}{\varepsilon_v - \varepsilon_n} + \frac{\Delta(wn)Z_K(nv)}{\varepsilon_w - \varepsilon_n}\right)(-1)^{J'} \begin{Bmatrix} J & J' & K \\ j_w & j_v & j_a \end{Bmatrix} \right. \\ & \left. +\delta(v,w) \left(\frac{Z_K(na)\Delta(cn)}{\varepsilon_c - \varepsilon_n} + \frac{\Delta(na)Z_K(cn)}{\varepsilon_a - \varepsilon_n}\right)(-1)^{J} \begin{Bmatrix} J & J' & K \\ j_c & j_a & j_v \end{Bmatrix}\right], \end{aligned} \tag{2}$$

$$\begin{aligned} & Z_K^{(\mathrm{RPA})}(av(J), cw(J')) = \frac{1}{2K+1}\sqrt{[J][J']}(-1)^{j_v+j_c} \\ & \times \left[\delta(c,a)(-1)^{J'} \begin{Bmatrix} J & J' & K \\ j_w & j_v & j_a \end{Bmatrix} \sum_{nb} \left[\frac{Z_K(nb)Z_K(wnvb)}{\varepsilon_b + \varepsilon_v - \varepsilon_w - \varepsilon_n} + \frac{Z_K(wbvn)Z_K(bn)}{\varepsilon_b + \varepsilon_w - \varepsilon_v - \varepsilon_n}\right] \right. \\ & \left. +\delta(w,v)(-1)^{J} \begin{Bmatrix} J & J' & K \\ j_c & j_a & j_v \end{Bmatrix} \sum_{nb} \left[\frac{Z_K(bn)Z_K(cban)}{\varepsilon_b + \varepsilon_c - \varepsilon_a - \varepsilon_n} + \frac{Z_K(cnab)Z_K(nb)}{\varepsilon_b + \varepsilon_a - \varepsilon_c - \varepsilon_n}\right], \end{aligned} \tag{3}$$

$$\begin{aligned} & Z_K^{(\mathrm{corr})}(av(J), cw(J')) = \sqrt{[J][J']} \\ & \times \left[\frac{1}{[J']} \sum_i \frac{Z_K(ai)Z_{J'}(cvwi)}{\varepsilon_i + \varepsilon_w - \varepsilon_c - \varepsilon_v}(-1)^{j_a - j_i + J + J'} \begin{Bmatrix} J & J' & K \\ j_i & j_a & j_v \end{Bmatrix} \right. \\ & +\frac{1}{[J']} \sum_i \frac{Z_{J'}(icaw)Z_K(iv)}{\varepsilon_i + \varepsilon_c - \varepsilon_a - \varepsilon_w}(-1)^{j_v - j_i + K} \begin{Bmatrix} J & J' & K \\ j_i & j_v & j_a \end{Bmatrix} \\ & \left. +\frac{1}{[J]} \sum_i \frac{Z_K(wi)Z_J(iacv)}{\varepsilon_i + \varepsilon_a - \varepsilon_c - \varepsilon_v}(-1)^{J + J' + K} \begin{Bmatrix} J & J' & K \\ j_w & j_i & j_c \end{Bmatrix}\right. \end{aligned}$$

$$+\frac{1}{[J]}\sum_i \frac{Z_J(awvi)Z_K(ic)}{\varepsilon_i+\varepsilon_v-\varepsilon_a-\varepsilon_w}\left\{\begin{array}{ccc} J & J' & K \\ j_c & j_i & j_w \end{array}\right\}\Bigg]. \quad (4)$$

In the above equations, the indexes a, b, c designate core states, n designates excited states, and i denotes an arbitrary core or excited state. In the sums over i in Eq. (4), all terms with vanishing denominators are excluded. $X_k(abcd)$ is the Coulomb matrix element. The definitions of $Z_k(abcd)$ and $\Delta(ij)$ are given by Eq.(2.3), Eq.(2.4), and Eq.(2.7) in Ref. [23], ε_i is the lowest order DF energy. The second-order reduced matrix element of the derivative term is given by

$$\begin{aligned} & Z_K^{(\mathrm{derv})}[av(J), cw(J')] \\ = \; & \alpha(E_{av}^{(1)} - E_{cw}^{(1)})\, P_K^{(\mathrm{derv})}[av(J), cw(J')]\,, \end{aligned} \quad (5)$$

where $E_{av}^{(1)}$ is the first-order correction to the energy defined by Eq.(2.2) in Ref. [23] and the quantity $P_K^{(\mathrm{derv})}$ is defined by

$$\begin{aligned} & P_K^{(\mathrm{derv})}(av(J), cw(J')) \\ = \; & \sqrt{[J][J']}(-1)^{K+j_v+j_c} \\ & \times\left[\delta(c,a)Z_K^{(\mathrm{derv})}(w,v)(-1)^{J'}\left\{\begin{array}{ccc} J & J' & K \\ j_w & j_v & j_a \end{array}\right\}\right. \\ & \left. +\delta(w,v)Z_K^{(\mathrm{derv})}(c,a)(-1)^{J}\left\{\begin{array}{ccc} J & J' & K \\ j_c & j_a & j_v \end{array}\right\}\right]. \end{aligned} \quad (6)$$

The expression for the K-pole $Z_K^{(\mathrm{derv})}(a,c)$ derivative term is obtained from $\omega\,\langle a\|\frac{dt_K^{(1)}}{d\omega}\|c\rangle$ and is given in Appendix A of Ref. [10]. In Eqs. (1)– (6), we use the K subscript to describe dipole transitions with $K = 1$, quadrupole transitions with $K = 2$, and octupole transitions with $K = 3$. Instead of using the K subscript, we use below additional number 1, 2, and 3 to identify dipole, quadrupole, and octupole transitions as E1, E2, and E3 transitions for electric-multipole transitions and as M1, M2, and M3 transitions for magnetic-multipole transitions.

All of the second-order correlation corrections that we discussed above result from the residual Coulomb interaction. To include correlation corrections due to the Breit interaction, the Coulomb matrix element $X_k(abcd)$ must be modified according to the rule

$$X_k(abcd) \to X_k(abcd) + M_k(abcd) + N_k(abcd), \quad (7)$$

where M_k and N_k are magnetic radial integrals defined by Eqs.(A4,A5) in Ref. [24].

We calculated electric-octupole (E3) matrix elements for the transitions between the 11 even-parity $3d_{5/2}4s_{1/2}(3)$, $3d_j4d_{j'}(3)$, $3p_{3/2}4p_{3/2}(3)$, $3p_j4f_{j'}(3)$, and $3s_{1/2}4d_{5/2}(2)$ excited states and the 13 odd-parity $3d_j4p_{j'}(1)$, $3d_j4f_{j'}(1)$, $3p_j4s_{1/2}(1)$, $3p_j4d_{j'}(1)$, and $3s_{1/2}4p_{j'}(1)$ excited states for Ni-like ions with nuclear charges $Z = 34-100$. For electric-quadrupole (E2) transitions, we calculated matrix elements for all possible transitions inside of even-parity complexes with $J = 1$, 2, and 3 (all together 650 lines) and inside of odd-parity complexes with $J = 0$–4 (all together 795 lines).

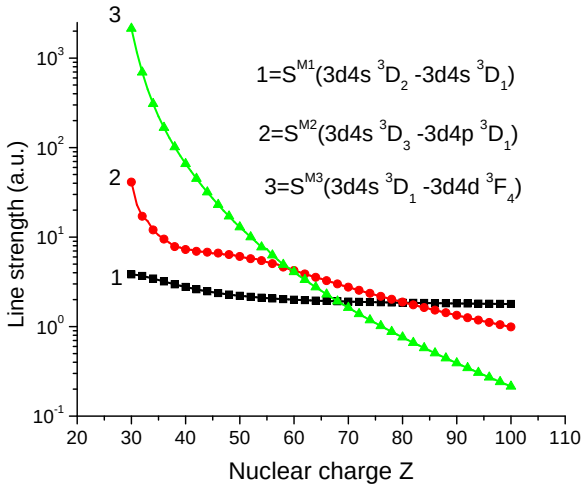

FIG. 1: Line strengths for M1, M2, and M3 transitions in Ni-like ions as a function of Z.

We calculated magnetic-quadrupole (M2) matrix elements for the transitions between the 11 even-parity $3d_{5/2}4s_{1/2}(3)$, $3d_j4d_{j'}(3)$, $3p_{3/2}4p_{3/2}(3)$, $3p_j4f_{j'}(3)$, and $3s_{1/2}4d_{5/2}(2)$ excited states and the 47 odd-parity excited states with $J = 1$, 2, 3, and 4. For magnetic-dipole (M1) and magnetic-octupole transitions, we calculated matrix elements for transitions inside of even-parity complexes with $J = 1$, 2, and 3. We considered transitions between states with $J = 2$ and states with $J = 1$, 2, and 3 in the case of M1 transitions (all together 518 transitions). In the case of M3 transitions, we considered the transitions between states with $J = 2$ and states with $J = 1$, 2, and 3 and, additionally, transitions between states with $J = 1$ and states with $J = 3$ and 2 (all together, 722 transitions).

A. Example: E2, E3, M1, M2, and M3 matrix elements for W^{46+}

In Table I, we list values of *uncoupled* first- and second-order E2 and E3 matrix elements $Z^{(1)}$, $Z^{(\mathrm{RPA})}$, $Z^{(\mathrm{corr})}$, $B^{(2)}$, together with derivative terms $P^{(\mathrm{derv})}$, for Ni-like tungsten, Z=74. We list values only for the six E2 transitions (among 1445 considered transitions) inside of $3d4s$ and $3d4p$ configurations and the three E3 transi-

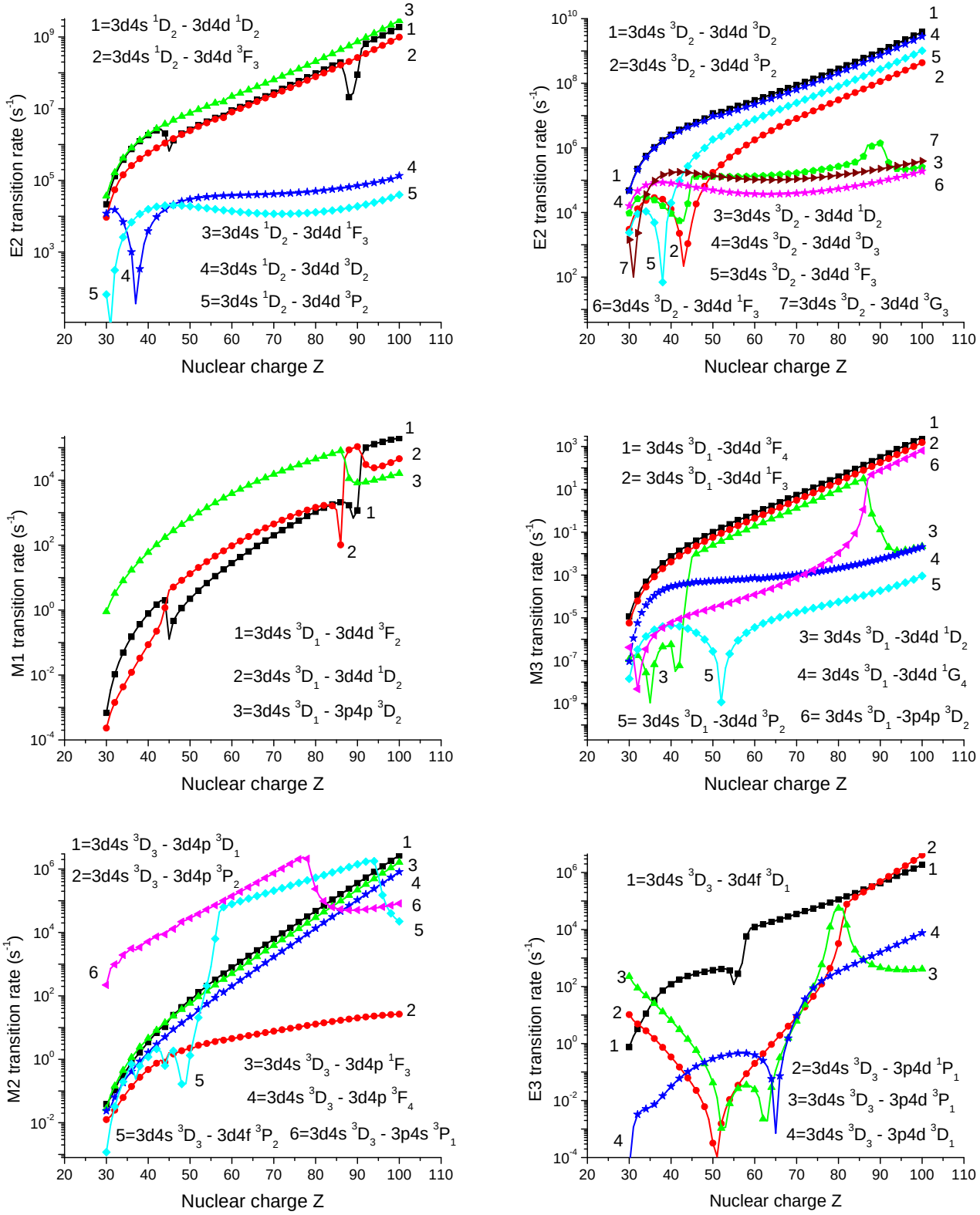

FIG. 2: E2, E3, M1, M2, and M3 transition rates in Ni-like ions as function of Z.

TABLE I: Contributions to E2 and E3 uncoupled reduced matrix elements (a.u.) in length L and velocity V forms for transitions between excited states $av(J)$ and $a'v'(J')$ in W^{46+}.

$av(J)$	$cw(J')$		$Z^{(1)}$	$Z^{(\mathrm{RPA})}$	$Z^{(\mathrm{corr})}$	$B^{(2)}$	$P^{(\mathrm{derv})}$
Electric-quadrupole transitions							
$3d_{3/2}4s_{1/2}(1)$	$3d_{5/2}4s_{1/2}(2)$	(L)	0.01607	-0.00074	-0.00016	-0.00004	0.03214
		(V)	-0.01585	0.00055	-0.00006	-0.00095	-0.01585
$3d_{3/2}4s_{1/2}(1)$	$3d_{5/2}4s_{1/2}(3)$	(L)	0.00859	-0.00040	-0.00009	-0.00002	0.01718
		(V)	-0.00847	0.00029	0.00003	-0.00061	-0.00847
$3d_{5/2}4s_{1/2}(2)$	$3d_{3/2}4s_{1/2}(2)$	(L)	-0.01052	0.00049	0.00004	0.00003	-0.02104
		(V)	-0.01038	-0.00036	0.00002	0.00074	0.01038
$3d_{5/2}4p_{3/2}(4)$	$3d_{5/2}4p_{1/2}(2)$	(L)	-0.19421	0.00144	0.00485	0.00052	-0.38839
		(V)	-0.19184	-0.00087	0.00011	-0.00117	-0.19179
$3d_{5/2}4p_{1/2}(3)$	$3d_{5/2}4p_{3/2}(1)$	(L)	0.13267	-0.00099	-0.00316	-0.00035	0.26532
		(V)	0.13105	0.00059	0.00564	0.00129	0.13102
$3d_{5/2}4p_{3/2}(2)$	$3d_{3/2}4p_{3/2}(0)$	(L)	0.01052	-0.00049	0.00010	-0.00002	0.02104
		(V)	-0.01038	0.00036	-0.00075	-0.00075	-0.01038
Electric-octupole transitions							
$3d_{5/2}4s_{1/2}(3)$	$3d_{5/2}4f_{5/2}(1)$	(L)	-0.04570	0.00005	0.00256	-0.00011	-0.13607
		(V)	-0.04559	0.00027	0.00310	-0.00001	-0.09118
$3d_{5/2}4s_{1/2}(3)$	$3p_{1/2}4s_{1/2}(1)$	(L)	-0.00739	0.00015	0.00004	-0.00003	-0.02063
		(V)	0.00664	0.00006	0.00003	-0.00002	0.01327
$3d_{5/2}4d_{3/2}(3)$	$3d_{5/2}4f_{5/2}(1)$	(L)	-0.03564	0.00005	0.00202	-0.00009	-0.10732
		(V)	-0.03624	0.00050	0.00249	0.00007	-0.07249

TABLE II: Contributions to M1,M2, and M3 uncoupled reduced matrix elements (a.u.) for transitions between excited states $av(J)$ and $cw(J')$ in W^{46+}.

$av(J)$	$cw(J')$	$Z^{(1)}$	$Z^{(\mathrm{RPA})}$	$Z^{(\mathrm{corr})}$	$B^{(2)}$	$P^{(\mathrm{derv})}$
Magnetic-dipole transitions						
$3d_{3/2}4s_{1/2}(1)$	$3d_{5/2}4s_{1/2}(2)$	1.33369	0.00004	0.00001	-0.00104	1.33369
$3d_{3/2}4s_{1/2}(1)$	$3d_{3/2}4s_{1/2}(2)$	-1.64902	-0.00044	0.00031	-0.00117	-1.64902
$3d_{5/2}4s_{1/2}(2)$	$3d_{5/2}4s_{1/2}(2)$	5.77997	-0.00152	0.00040	-0.00669	5.77997
$3d_{5/2}4s_{1/2}(2)$	$3d_{3/2}4s_{1/2}(2)$	-0.44456	-0.00001	0.00000	0.00037	-0.44456
$3d_{5/2}4s_{1/2}(2)$	$3d_{5/2}4s_{1/2}(3)$	-1.37260	-0.00039	0.00039	-0.00125	-1.37260
Magnetic-quadrupole transitions						
$3d_{5/2}4s_{1/2}(3)$	$3d_{5/2}4p_{3/2}(1)$	-1.48523	-0.00185	0.01413	0.00140	-2.97027
$3d_{5/2}4s_{1/2}(3)$	$3p_{3/2}4s_{1/2}(1)$	0.48761	0.00768	-0.00407	-0.00064	0.97514
$3d_{5/2}4s_{1/2}(3)$	$3p_{1/2}4s_{1/2}(1)$	-0.54676	-0.01110	-0.00071	0.00082	-1.09327
$3d_{5/2}4d_{3/2}(3)$	$3d_{5/2}4f_{5/2}(1)$	0.34721	-0.00079	-0.00354	-0.00020	0.69442
$3d_{5/2}4d_{3/2}(3)$	$3d_{5/2}4f_{7/2}(1)$	-0.07815	-0.00031	0.00228	-0.00002	-0.15628
Magnetic-octupole transitions						
$3d_{3/2}4s_{1/2}(1)$	$3d_{5/2}4s_{1/2}(3)$	-0.01921	0.00034	0.00039	-0.00002	-0.05764
$3d_{5/2}4s_{1/2}(2)$	$3d_{5/2}4s_{1/2}(2)$	-0.23651	0.00132	-0.00118	-0.00025	-0.70954
$3d_{5/2}4s_{1/2}(2)$	$3d_{5/2}4s_{1/2}(3)$	-0.19311	0.00108	-0.00135	-0.00020	-0.57934
$3d_{3/2}4s_{1/2}(2)$	$3d_{5/2}4s_{1/2}(3)$	-0.02578	0.00045	-0.00053	-0.00002	-0.07733
$3d_{5/2}4d_{5/2}(1)$	$3s_{1/2}4d_{5/2}(3)$	0.17372	0.00253	0.00746	0.00040	0.52105

TABLE III: E2 and E3 coupled reduced matrix elements Q calculated in length L and velocity V forms for W^{46+}.

		First order		RMBPT		$3l_14l_2$	$3l_34l_4$
$av(J)$	$cw(J)$	L	V	L	V	$^{1,3}L_J$	$^{1,3}L'_{J'}$
Electric-quadrupole transitions							
$3d_{3/2}4s_{1/2}(1)$	$3d_{5/2}4s_{1/2}(3)$	-0.00962	-0.00742	-0.00910	-0.00801	$3d4s\ ^3D_1$	$3d4s\ ^3D_3$
$3d_{3/2}4s_{1/2}(2)$	$3d_{5/2}4s_{1/2}(3)$	0.02304	0.01834	0.02138	0.01963	$3d4s\ ^1D_2$	$3d4s\ ^3D_3$
$3d_{5/2}4s_{1/2}(2)$	$3d_{5/2}4s_{1/2}(3)$	-0.02018	-0.00162	-0.00966	-0.00841	$3d4s\ ^3D_2$	$3d4s\ ^3D_3$
$3d_{3/2}4d_{3/2}(2)$	$3d_{3/2}4s_{1/2}(2)$	-0.14491	-0.14504	-0.13922	-0.13976	$3d4d\ ^3F_2$	$3d4s\ ^1D_2$
$3d_{5/2}4d_{3/2}(2)$	$3d_{5/2}4s_{1/2}(3)$	0.16094	0.16128	0.15466	0.15647	$3d4d\ ^1D_2$	$3d4s\ ^3D_3$
$3d_{3/2}4d_{3/2}(3)$	$3d_{3/2}4s_{1/2}(1)$	0.16569	0.16475	0.16049	0.15950	$3d4d\ ^1F_3$	$3d4s\ ^3D_1$
$3d_{3/2}4p_{1/2}(1)$	$3d_{3/2}4p_{3/2}(3)$	-0.16506	-0.16029	-0.16815	-0.16964	$3d4p\ ^3P_1$	$3d4p\ ^3D_3$
$3d_{5/2}4p_{1/2}(2)$	$3d_{3/2}4p_{1/2}(2)$	0.07392	0.07756	0.06909	0.07012	$3d4p\ ^3F_2$	$3d4p\ ^1D_2$
$3d_{3/2}4p_{1/2}(1)$	$3d_{3/2}4p_{3/2}(1)$	-0.03937	-0.04409	-0.03542	-0.03818	$3d4p\ ^3P_1$	$3d4p\ ^1P_1$
Electric-octupole transitions							
$3d_{5/2}4s_{1/2}(3)$	$3p_{1/2}4s_{1/2}(1)$	0.00745	0.00636	0.00700	0.00671	$3d4s\ ^3D_3$	$3p4s\ ^3P_1$
$3d_{5/2}4s_{1/2}(3)$	$3s_{1/2}4p_{3/2}(1)$	0.00021	0.00007	0.00337	0.00294	$3d4s\ ^3D_3$	$3s4p\ ^1P_1$
$3d_{5/2}4d_{5/2}(3)$	$3d_{5/2}4f_{5/2}(1)$	-0.00125	-0.00138	-0.00427	-0.00405	$3d4d\ ^3D_3$	$3d4f\ ^3P_1$
$3d_{5/2}4d_{3/2}(3)$	$3d_{3/2}4f_{5/2}(1)$	-0.01952	-0.02028	-0.02158	-0.02210	$3d4d\ ^3G_3$	$3d4f\ ^1P_1$
$3d_{5/2}4d_{3/2}(3)$	$3p_{3/2}4s_{1/2}(1)$	-0.00565	-0.00613	-0.00914	-0.00928	$3d4d\ ^3G_3$	$3p4s\ ^1P_1$
$3d_{3/2}4d_{3/2}(3)$	$3p_{3/2}4s_{1/2}(1)$	0.01751	0.01794	0.01657	0.01659	$3d4d\ ^3F_3$	$3p4s\ ^1P_1$

tions (among 143 considered transitions) between even-parity states with $J = 3$ and odd-parity states with $J = 1$, respectively. Matrix elements in both length (L) and velocity (V) forms are given. We can see that the first-order matrix elements, $Z_L^{(1)}$ and $Z_V^{(1)}$, differ by 2–10%; however, the L–V differences between second-order matrix elements ($Z^{(\mathrm{RPA})}$, $Z^{(\mathrm{corr})}$, $B^{(2)}$) are much larger for some transitions. It can be also seen from Table I that for the E2 transition, the derivative term in velocity form, $P^{(\mathrm{derv})}$, almost equals $Z^{(1)}$ in velocity form and the derivative term, $P^{(\mathrm{derv})}$, in length form is larger by factor of two than $Z^{(1)}$ in length form (see, for example, Eqs. (A19)- (A22) [10]). For the E3 transition, the ratio of the $P^{(\mathrm{derv})}$ and $Z^{(1)}$ values is equal to almost two in length form and to three in velocity form.

In Table I, we present only one-electron transitions allowed in the first-order approximation, however, for most transitions the value of $Z^{(1)}$ is equal to zero. It should be noted, that the second-order contribution $Z^{(\mathrm{RPA})}$ has the same angular part as the first-order $Z^{(1)}$ contribution (compare Eqs. (3) and (1)). As a result, we have a non-zero contribution for the two-particle transitions only for second-order correlation contribution $Z^{(\mathrm{corr})}$, given by Eq. (4).

In Table II, we list values of *uncoupled* first- and second-order M1, M2, and M3 matrix elements $Z^{(1)}$, $Z^{(\mathrm{RPA})}$, $Z^{(\mathrm{corr})}$, and $B^{(2)}$ together with derivative terms $P^{(\mathrm{derv})}$ for Ni-like tungsten, Z=74. We list values only for the five one-electron $3d_j4s\ (J) - 3d_{j'}4s\ (J')$ magnetic-dipole transitions (among 518 considered transitions). We list similar matrix elements for M3 transitions in Table II. A comparison of the results given in this table for M1 and M3 transitions shows that the values of $Z^{(1)}$ for the M1 transitions are larger than the values of $Z^{(1)}$ for the M3 transitions by a factor of 10–100. The derivative term in a given M1 transition, $P^{(\mathrm{derv})}$, is almost equal to the first-order contribution $Z^{(1)}$, however, the derivative term in a given M3 transition, $P^{(\mathrm{derv})}$, is larger than the first-order contribution $Z^{(1)}$, by a factor of 3.

The five M2 transitions listed in Table II illustrate transitions between the even-parity states with $J = 3$ and odd-parity states with $J = 1$. The largest value of $Z^{(1)}$ is for the $3d_{5/2}4s_{1/2}(3) - 3d_{5/2}4p_{3/2}(1)$ transition, the smallest value of $Z^{(1)}$ is for the $3d_{5/2}4d_{3/2}(3) - 3d_{5/2}4f_{7/2}(1)$ transition. There are no large differences in the one-electron matrix elements ($Z_2(4p_{3/2}4s_{1/2}) =$ -1.775197, $Z_2(4f_{7/2}4d_{3/2}) =$ -1.307818), however, the angular factors in Eq. (1) are very different (0.182574 and 0.013041, respectively). We already mentioned the importance of two-electron transitions since their non-zero contribution is due to second-order correlation matrix elements $Z^{(\mathrm{corr})}$ defined by Eq. (4). The ratio of two-electron and one-electron transitions is equal to 3; there are 367 two-electron and 130 one-electron transitions among the 517 M2 transitions considered here.

B. E2, E3, M1, M2, and M3 Coupled Matrix Elements

The coupled transition matrix element between the initial eigenstate I with angular momentum J and the final state F with angular momentum J' is given by:

$$Q_K^{(1+2)}(I-F) = \frac{1}{E_K^I - E_K^F} \sum_{av} \sum_{cw} C_1^I(av) C_1^F(cw)$$

$$\times \Big\{ [\varepsilon_{av} - \varepsilon_{cw}] \left[ZB_K^{(1+2)}[av(J) - cw(J')] \right] + \left[E_1^I - E_1^F - \varepsilon_{av} + \varepsilon_{cw} \right] P_K^{(\mathrm{derv})}[av(J) - cw(J')] \Big\} . \quad (8)$$

Here, $\varepsilon_{av} = -\varepsilon_a + \varepsilon_v$ and $ZB_K^{(1+2)} = Z_K^{(1)} + Z_K^{(\mathrm{DF})} + Z_K^{(\mathrm{RPA})} + Z_K^{(\mathrm{corr})} + B_K^{(\mathrm{DF})} + B_K^{(\mathrm{RPA})} + B_K^{(\mathrm{corr})}$. The mixing coefficients $C_1^I(av)$, $C_1^F(cw)$ and energies E_K^I, E_K^I are obtained by diagonalizing the first-order effective Hamiltonian which includes both Coulomb and Breit interactions [23]. The energy terms E_K^I and E_K^F are defined as the sum of the DF energies $E^{(0)}$and the first-order energies $E^{(1)}$ obtained after diagonalization [23] of the initial I and final F states: $E_K = E^{(0)} + KE^{(1)}$. Using these formulas together with the uncoupled reduced matrix elements given in Tables I and II, we transform the uncoupled matrix elements to matrix elements between coupled (physical) states.

Values of E2 and E3 *coupled* reduced matrix elements in length and velocity forms are given in Table III for the transitions considered in Table I. Although we use an intermediate-coupling scheme, it is nevertheless convenient to label the physical states using the jj labelling for high Z and the LS labelling for low Z; both designations are used in Table III. The third and fourth columns in Table III show L and V values of *coupled* reduced matrix elements calculated in first-order RMBPT. The $L-V$ difference is about 5–10% for most cases, except $3d_j 4s_{1/2}(J) - 3d_{j'} 4s_{1/2}(J')$ transitions. Including the second-order contributions (columns with 'RMBPT' heading in Table III) decreases the $L-V$ difference to 0.2-2%. This non-zeroth $L-V$ difference arises because we start our RMBPT calculations using a non-local Dirac-Fock (DF) potential. If we were to replace the DF potential by a local potential, the differences would disappear completely. It should be emphasized that we include the negative energy state (NES) contributions to sums over intermediate states (see Ref. [11, 12] for details). Neglecting the NES contributions leads only to small changes in the L-form matrix elements but to substantial changes in some of the V-form matrix elements with a consequent loss of gauge independence.

A qualitative difference between the E2 and E3 transitions is that E2 transitions can occur between states with av=cw while the corresponding E3 transitions are forbidden. In such cases we obtain for $Q_K^{(1+2)}(I-F)$ from Eq. (8):

$$Q_K^{(1+2)}(I-F) = \frac{1}{E_K^I - E_K^F} \sum_{av} \sum_{cw} C_1^I(av) C_1^F(av) \times \left[E_1^I - E_1^F \right] P_K^{(\mathrm{derv})}[av(J) - av(J')]. \quad (9)$$

It was already mentioned that the value of $P_L^{(\mathrm{derv})}$ in length form is larger by a factor of 2 than the value of $P_V^{(\mathrm{derv})}$ in velocity form. As a result, there are huge differences between transition amplitudes calculated in length and velocity forms. These differences are compensated by the velocity form of the second-order diagram $Z^{(\mathrm{corr})}$ [25]

$$Z^{(\mathrm{corr})}[av(J) - av(J')] = \frac{1}{\omega} \left[E_1^I - E_1^F \right] P_V^{(\mathrm{derv})}[av(J) - av(J')], \quad (10)$$

where ω is the photon energy, which should be equal to zero in our case. For practical calculations, we use $\omega = 10^{-7}$. We use the same value of 10^{-7} for $[\varepsilon_{av} - \varepsilon_{cw}]$ in Eq. (8). As a result, we obtain an additional contribution to the transition amplitude in the velocity form; however, the $L-V$ difference is larger than for transitions with different av and cw states (see Table III).

In Fig. 1, we illustrate the Z-dependence of the line strengths of M1, M2, and M3 transitions from the $3d4s\ ^3D_J$ excited state to other excited states in Ni-like sequence. Those line strengths are obtained as a square of coupled matrix elements given by Eq. (8). We can see from Fig. 1 that the largest value of the line strengths is for the M3 $3d4s\ ^3D_1 - 3d4d\ ^3F_4$ transition for small-Z ions. However, for high-Z ions, the value of $S^{M3}(3d4s\ ^3D_1 - 3d4d\ ^3F_4)$ becomes the smallest one. The opposite behavior among the three curves '1' – '3' shown in Fig. 1 is seen for the curve '1' describing the M1 $3d4s^3D_2 - 3d4s^3D_1$ transition. The value of $S^{M1}(3d4s\ ^3D_2 - 3d4s\ ^3D_1)$ becomes the smallest for the low-Z ions and the largest for high-Z ions. The value of the $3d4s\ ^3D_2 - 3d4s\ ^3D_1$ M1 transition is almost constant with Z, as was shown previously in Ref. [26]. The leading term for the line strength of M2 transitions was found in [27] to be proportional to $\sim 1/Z^2$. Following the procedure given in [27], we find that the leading term for the line strengths of M3 transitions is proportional to $\sim 1/Z^4$. We find that the value of $S^{M3}(3d4s\ ^3D_1 - 3d4d\ ^3F_4)$ is proportional to $\frac{A}{(Z-21)^4}$ with A changing very smoothly from 8.4×10^6 to 9.4×10^6 for almost the entire range of Z (Z =34–100) and the value of $S^{M2}(3d4s\ ^3D_3 - 3d4p\ ^3D_1)$ is proportional to $\frac{A}{(Z-21)^2}$ with A changing very smoothly from 6.2×10^3 to 6.5×10^3 for the range of Z =52–100). The fact that the screening factor is equal to 21 confirms the leading terms discussed above. This screening factor was used previously in [11, 12].

III. RESULTS AND DISCUSSION

We calculated the line strengths and transition rates for numerous transitions between and inside the $3s^23p^63d^94l$, $3s^23p^53d^{10}4l$, and $3s3p^63d^{10}4l$ levels (with $4l = 4s$, $4p$, $4d$, and $4f$) and the ground state in Ni-like ions with the nuclear charges ranging from $Z = 34$ to 100. The number of such transitions increases dramatically compared to transitions from the $3s^23p^63d^94l$, $3s^23p^53d^{10}4l$, and $3s3p^63d^{10}4l$ states (with $4l = 4s$, $4p$, $4d$, and $4f$) into the ground state [10, 11]. For M2 and

TABLE IV: Wavelengths (λ in Å) and transition rates (A_r in s^{-1}) for E2, M1 and M3 transitions in Ni-like W^{46+}.

Transitions		λ	A_r	Transitions		λ	A_r	Transitions		λ	A_r
E2 transitions				M1 transitions				M3 transitions			
$3d4s\ ^3D_3$	$3d4s\ ^1D_2$	182.96	4.994[2]	$3d4s\ ^3D_3$	$3d4s\ ^1D_2$	182.96	2.34[6]	$3d4s\ ^3D_2$	$3s4s\ ^3S_1$	12.438	1.59[3]
$3d4s\ ^3D_3$	$3d4s\ ^3D_1$	186.24	1.379[2]	$3d4s\ ^3D_2$	$3d4s\ ^1D_2$	187.89	1.63[5]	$3d4s\ ^3D_3$	$3s4s\ ^3S_1$	12.415	1.16[3]
$3d4s\ ^3D_2$	$3d4s\ ^1D_2$	187.89	9.051[1]	$3d4s\ ^3D_2$	$3d4s\ ^3D_1$	191.35	2.41[6]	$3d4d\ ^3S_1$	$3s4d\ ^3D_2$	12.373	5.73[2]
$3d4s\ ^3D_2$	$3d4s\ ^3D_1$	191.35	4.749[2]	$3d4s\ ^3D_3$	$3d4s\ ^3D_2$	6976.3	3.18[1]	$3d4d\ ^3D_1$	$3s4d\ ^3D_3$	12.406	3.85[2]
$3d4s\ ^3D_1$	$3d4d\ ^1D_2$	33.325	1.077[8]	$3d4s\ ^3D_1$	$3d4s\ ^1D_2$	10394.	1.24[1]	$3d4d\ ^3P_2$	$3s4d\ ^3D_2$	12.448	7.81[2]
$3d4s\ ^3D_2$	$3d4d\ ^3D_3$	33.445	9.830[7]	$3d4s\ ^3D_1$	$3d4d\ ^1D_2$	173.30	3.14[5]	$3d4d\ ^3D_2$	$3s4d\ ^3D_3$	12.490	5.26[2]
$3d4s\ ^1D_2$	$3d4d\ ^1F_3$	33.270	9.901[7]	$3d4d\ ^3P_2$	$3d4d\ ^3F_2$	176.62	5.81[5]	$3d4d\ ^3G_3$	$3s4d\ ^3D_1$	12.493	8.55[2]
$3d4s\ ^3D_2$	$3d4s\ ^3D_1$	33.941	1.419[8]	$3d4d\ ^3D_2$	$3d4d\ ^1D_2$	191.38	9.59[5]	$3d4d\ ^3G_3$	$3s4d\ ^3D_2$	12.475	8.32[2]
$3d4s\ ^3D_3$	$3d4d\ ^3S_1$	36.118	1.042[8]	$3d4d\ ^3D_2$	$3d4d\ ^1F_3$	186.19	1.44[5]	$3d4d\ ^3D_3$	$3s4d\ ^1D_2$	12.462	4.11[2]
$3d4s\ ^3D_3$	$3d4d\ ^3P_2$	35.495	9.509[7]	$3d4d\ ^3P_2$	$3d4d\ ^3D_1$	193.06	1.64[6]	$3d4s\ ^3D_2$	$3d4d\ ^3P_2$	35.676	1.06[-2]
$3d4p\ ^3F_2$	$3d4p\ ^3F_4$	120.25	2.007[5]	$3d4d\ ^3D_2$	$3d4d\ ^3P_1$	206.50	6.87[5]	$3d4s\ ^3D_2$	$3d4d\ ^3D_2$	33.324	2.73[0]
$3d4p\ ^3F_3$	$3d4p\ ^1D_2$	119.40	2.103[5]	$3d4d\ ^3S_1$	$3d4d\ ^3F_2$	162.65	5.16[4]	$3d4s\ ^1D_2$	$3d4d\ ^3D_2$	40.509	4.14[-3]
$3d4p\ ^3F_3$	$3d4p\ ^3D_1$	118.22	2.773[5]	$3d4d\ ^3P_2$	$3d4d\ ^3F_3$	191.89	1.96[4]	$3d4s\ ^3D_2$	$3d4d\ ^3F_2$	29.681	1.36[-2]
$3d4p\ ^3P_2$	$3d4p\ ^3P_0$	124.13	2.262[5]	$3d4d\ ^3G_3$	$3d4d\ ^3F_2$	182.27	1.88[6]	$3d4s\ ^3D_2$	$3d4d\ ^1D_2$	28.382	8.14[-2]
$3d4p\ ^3P_2$	$3d4p\ ^1P_1$	118.98	2.493[5]	$3d4d\ ^3D_3$	$3d4d\ ^1D_2$	187.50	1.19[6]	$3d4s\ ^1D_2$	$3d4d\ ^1D_2$	33.432	1.53[1]

TABLE V: Energies (ΔE in eV) and radiative rates (A_r in s^{-1}) for M1 and E2 transitions inside of $3d4s$ and $3d4p$ configurations in Ni-like U^{64+}, Th^{62+}, Bi^{55+}, and Hg^{52+}. The RMBPT results (a) are compared with MCDF results (b) given by Biémont [5].

Transitions			U^{64+}, $Z=92$		Th^{62+}, $Z=90$		Bi^{55+}, $Z=83$		Hg^{52+}, $Z=80$	
			ΔE	A_r	ΔE	A_r	ΔE	A_r	ΔE	A_r
Magnetic-dipole transitions										
$3d_{5/2}4s_{1/2}(3)$	$3d_{3/2}4s_{1/2}(2)$	(a)	190.93	5.29[7]	172.18	3.88[7]	117.37	1.23[7]	98.50	7.23[6]
		(b)	189.83	5.21[7]	171.15	3.82[7]	116.64	1.21[7]	97.86	7.11[6]
$3d_{5/2}4s_{1/2}(2)$	$3d_{3/2}4s_{1/2}(1)$	(a)	186.80	5.56[7]	168.18	4.07[7]	113.85	1.28[7]	95.17	7.52[6]
		(b)	185.58	5.46[7]	167.06	4.00[7]	113.03	1.25[7]	94.45	7.36[6]
$3d_{5/2}4s_{1/2}(2)$	$3d_{3/2}4s_{1/2}(2)$	(a)	188.34	3.73[6]	169.68	2.73[6]	115.21	8.61[5]	96.47	5.07[5]
		(b)	187.08	3.66[6]	168.52	2.68[6]	114.36	8.43[5]	95.72	4.96[5]
Electric-quadrupole transitions										
$3d_{5/2}4p_{1/2}(2)$	$3d_{5/2}4p_{3/2}(4)$	(a)	327.69	1.72[7]	291.10	1.09[7]	189.04	2.05[6]	155.58	9.70[5]
		(b)	326.98	1.63[7]	290.35	1.02[7]	188.29	1.88[6]	154.86	8.76[5]
$3d_{5/2}4p_{1/2}(2)$	$3d_{3/2}4p_{1/2}(2)$	(a)	330.08	4.56[6]	293.45	2.86[6]	191.23	5.19[5]	157.69	2.27[5]
		(b)	329.95	4.82[6]	293.24	3.02[6]	190.85	5.52[5]	157.29	2.56[5]
$3d_{5/2}4p_{1/2}(2)$	$3d_{5/2}4p_{3/2}(1)$	(a)	331.62	1.48[6]	294.95	9.31[5]	192.53	1.70[5]	158.91	9.14[4]
		(b)	331.77	1.57[6]	294.99	9.84[5]	192.39	1.79[5]	158.73	
$3d_{5/2}4p_{1/2}(2)$	$3d_{5/2}4p_{3/2}(3)$	(a)	334.62	1.05[7]	297.81	6.64[6]	194.98	1.27[6]	161.20	6.04[5]
		(b)	333.93	1.03[7]	297.09	6,52[6]	194.26	1.23[6]	160.51	5.79[5]

E3 transitions, we need to consider transitions between levels of different parity, however, for M1, E2, and M3 transitions, we need to consider transitions between levels of the same parity. That involves transitions not only between different configurations, but also transitions inside the same configuration.

Line strengths and transition rates for the 517 M2 transitions between even-parity states with J=3 and odd-parity states with J=1–4 were evaluated. For the 143 E3 transitions, we considered transitions between even-parity states with J=3 and odd-parity states with J=1, only. We calculated line strengths and transition rates for the 518 M1, E2, and M3 transitions between even-parity $[J=1,2] \leftrightarrow [J=2]$ and $[J=2] \leftrightarrow [J=3]$ complexes. In addition, the atomic properties for the 132 E2 and M3 transitions between even-parity $[J=1] \leftrightarrow [J=3]$ complexes and the 72 M3 transitions between even-parity $[J=1] \leftrightarrow [J=4]$ complexes were evaluated. The atomic properties for all allowed and forbidden E2 lines between odd-parity complexes were calculated as well. The results for electric-multipole transitions were calculated in both length and velocity forms but, since the L form is less sensitive to various contributions, only the length-form results are presented in the tables and figures presented here. The theoretical energies used to evaluate transition rates were calculated using the second-order RMBPT.

TABLE VI: Wavelengths (λ in Å) and transition rates (A_r in s^{-1}) for the $3d4s\ ^3D_2 - 3d4s\ ^3D_1$ M1 transitions in Ni-like ions, evaluated in first-order (RMBPT-I) and second-order RMBPT (RMBPT-II).

	RMBPT-I		RMBPT-II			RMBPT-I		RMBPT-II	
Z	λ	A_r	λ	A_r	Z	λ	A_r	λ	A_r
34	20034.	3.84[0]	22292.	2.79[0]	68	292.78	6.88[5]	292.78	6.87[5]
35	16099.	7.13[0]	17403.	5.66[0]	69	271.89	8.55[5]	271.85	8.55[5]
36	13063.	1.29[1]	14016.	1.04[1]	70	252.83	1.06[6]	252.74	1.06[6]
37	10701.	2.25[1]	11479.	1.83[1]	71	235.42	1.31[6]	235.33	1.31[6]
38	8847.0	3.85[1]	9247.5	3.37[1]	72	219.48	1.61[6]	219.38	1.61[6]
39	7377.9	6.41[1]	7642.6	5.77[1]	73	204.88	1.97[6]	204.76	1.97[6]
40	6203.0	1.04[2]	6417.7	9.43[1]	74	191.47	2.41[6]	191.35	2.41[6]
41	5254.9	1.66[2]	5454.9	1.49[2]	75	179.13	2.93[6]	178.95	2.94[6]
42	4483.1	2.60[2]	4509.8	2.56[2]	76	167.78	3.56[6]	167.61	3.57[6]
43	3849.9	4.00[2]	3937.4	3.74[2]	77	157.31	4.31[6]	157.15	4.32[6]
44	3326.2	6.06[2]	3346.4	5.95[2]	78	147.64	5.20[6]	147.49	5.21[6]
45	2889.9	9.02[2]	2925.8	8.70[2]	79	138.71	6.26[6]	138.55	6.27[6]
46	2524.1	1.33[3]	2569.7	1.26[3]	80	130.44	7.50[6]	130.28	7.52[6]
47	2215.3	1.92[3]	2239.1	1.86[3]	81	122.77	8.98[6]	122.61	9.00[6]
48	1953.1	2.76[3]	1966.3	2.70[3]	82	115.66	1.07[7]	115.50	1.07[7]
49	1729.2	3.91[3]	1729.3	3.90[3]	83	109.05	1.28[7]	108.90	1.28[7]
50	1537.0	5.48[3]	1561.7	5.22[3]	84	102.91	1.52[7]	102.76	1.52[7]
51	1371.2	7.61[3]	1387.1	7.35[3]	85	97.19	1.80[7]	97.04	1.80[7]
52	1227.4	1.05[4]	1237.3	1.02[4]	86	91.86	2.12[7]	91.71	2.13[7]
53	1102.3	1.43[4]	1110.8	1.40[4]	87	86.89	2.50[7]	86.74	2.51[7]
54	993.02	1.93[4]	1004.8	1.86[4]	88	82.25	2.95[7]	82.11	2.96[7]
55	897.10	2.60[4]	882.36	2.72[4]	89	77.91	3.46[7]	77.77	3.47[7]
56	812.62	3.46[4]	812.93	3.45[4]	90	73.85	4.06[7]	73.72	4.07[7]
57	737.98	4.58[4]	738.55	4.56[4]	91	70.05	4.75[7]	69.93	4.76[7]
58	671.81	6.02[4]	668.99	6.08[4]	92	66.49	5.54[7]	66.37	5.56[7]
59	612.98	7.87[4]	614.31	7.81[4]	93	63.15	6.46[7]	63.04	6.48[7]
60	560.50	1.02[5]	561.25	1.02[5]	94	60.02	7.51[7]	59.91	7.54[7]
61	513.58	1.32[5]	514.02	1.31[5]	95	57.08	8.72[7]	56.97	8.76[7]
62	471.51	1.70[5]	471.94	1.69[5]	96	54.31	1.01[8]	54.21	1.02[8]
63	433.69	2.17[5]	433.87	2.16[5]	97	51.71	1.17[8]	51.61	1.17[8]
64	399.61	2.75[5]	400.10	2.74[5]	98	49.26	1.35[8]	49.16	1.36[8]
65	368.84	3.48[5]	369.04	3.48[5]	99	46.95	1.56[8]	46.86	1.57[8]
66	340.99	4.39[5]	341.11	4.38[5]	100	44.78	1.79[8]	44.68	1.80[8]
67	315.73	5.51[5]	315.79	5.50[5]					

A. E2, E3, M1, M2, and M3 transition rates

The general trends of the Z dependence of the transition rates for the E2, M2, E3, M1, E2, and M3 transitions are presented in Fig. 2 for Ni-like ions with nuclear charge $Z = 30 - 100$.

The E1, E2, E3, M1, M2, and M3 transition probabilities A_r (s^{-1}) for the transitions between the $3l_14l_2$ LSJ and $3l_34l_4$ $L'S'J'$ excited states are obtained in terms of line strengths S (a.u.) and wavelength λ(Å) as

$$A_r(EK) = \frac{A_K S^{(EK)}}{(2J+1)\lambda^{2K+1}}, \quad A(MK) = \frac{B_K S^{(MK)}}{(2J+1)\lambda^{2K+1}} \tag{11}$$

The factors A_K are equal to $2.02613\times\ 10^{18}$, $1.11995\times\ 10^{18}$, and $3.14441\times\ 10^{17}$, and the factors B_K are equal to $2.69735\times\ 10^{13}$, $1.49097\times\ 10^{13}$, and $4.18610\times\ 10^{12}$ for K=1, 2, and 3, respectively.

From the many multipole transitions, we choose transitions with initial $3d4s\ ^{1,3}D_J$ levels. We obtain the 47 M2 transitions between $3d4s\ ^3D_3$ and odd-parity levels with J=1–4. The number of E3 transitions from $3d4s\ ^3D_3$ state to odd-parity levels with J=1 is equal to 13. As a result, we decrease the number of transitions by a factor of 10. Some of those transitions are illustrated in Fig. 2.

Transition rates for the five E2 lines from the $3d4s\ ^1D_2$ level and the seven E2 lines from $3d4s\ ^3D_2$ level to the $3d4d\ ^{1,3}L_J$ levels are plotted in the two top panels of Fig. 2. The curves describing the $3d4s\ ^1D_2 - 3d4d\ ^{1,3}F_3$ and the $3d4s\ ^3D_2 - 3d4d\ ^3D_J$ transition rates smoothly increase with Z without any sharp features. The difference in values of A_r for $3d4s\ ^3D_2 - 3d4d\ ^3D_2$ and $3d4s\ ^3D_2 - 3d4d\ ^3D_3$ lines is about 20–50%. The two minima at Z= 45 and Z= 88-89 for the curve labeled '1'=$3d4s\ ^1D_2 - 3d4d\ ^1D_2$ can be explained by the mixing of the $3d_{3/2}4d_{3/2}$ (2), $3d_{3/2}4d_{5/2}$ (2), and $3p_{3/2}4p_{1/2}$ (2) states [11]. We can see from the curves shown on the left top panel of Fig. 2 that there is a large difference in the

values of A_r for transitions described by curves 1, 2, 3 and 4, 5, respectively. This difference is due to the type of transitions: one-electron and two-electron in the first and second case, respectively. The same explanation applies to the differences of the A_r values for the transitions describing by curves 1, 2, 4, 5 and 3, 6, 7, respectively, shown on the right top panel of Fig. 2.

The three M1 lines from the $3d4s\ ^3D_1$ level illustrated the 26 possible M1 transitions in the left central panel of Fig. 2. The sharp features seen in the curves describing the $3d4s\ ^3D_1 - 3d4d\ ^3F_2$ and $3d4s\ ^3D_1 - 3d4d\ ^1D_2$ transitions can be explained by a change of the dominant contribution in the mixing coefficients for the $3d4d\ ^3F_2$ ($3d_{3/2}4d_{5/2}(2)$ for Z = 30–44, $3d_{3/2}4d_{5/2}(2)$ for Z = 45–90, and $3p_{3/2}4p_{1/2}(2)$ for Z = 91–100) and $3d4d\ ^1D_2$ ($3d_{3/2}4d_{3/2}(2)$ for Z = 30–44, $3d_{3/2}4d_{5/2}(2)$ for Z=45–86, $3p_{3/2}4p_{1/2}(2)$ for Z = 87–90, and $3d_{3/2}4d_{3/2}(2)$ for Z = 91–100) levels.

The six M3 lines from the $3d4s\ ^3D_1$ level illustrate the 48 possible M3 transitions in the right central panel of Fig. 2. The curves describing '1'=$3d4s\ ^3D_1 - 3d4d\ ^3F_4$, '2'=$3d4s\ ^3D_1 - 3d4d\ ^1F_3$, and '4'=$3d4s\ ^3D_1 - 3d4d\ ^3G_4$, transition rates smoothly increase with Z without any sharp features. We notice that mixing coefficients for those states are almost equal to 1. As a result, we can rewrite those coupled states as uncoupled states, as '1'=$3d_{3/2}4s_{1/2}(1) - 3d_{3/2}4d_{5/2}(4)$, '2'=$3d_{3/2}4s_{1/2}(1) - 3d_{3/2}4d_{5/2}(3)$, and '4'=$3d_{3/2}4s_{1/2}(1) - 3d_{5/2}4d_{3/2}(4)$. As can be seen from the curves shown in the right central panel of Fig. 2, the curves with labels '1' and '2' are almost coincident; however, the values of A_r for the curve with label '4' are smaller by two orders of magnitude than the values of A_r for the curves with labels '1' and '2'. We already mentioned previously the difference in values of A_r for two-electron transitions (4'=$3d_{3/2}4s_{1/2}(1) - 3d_{5/2}4d_{3/2}(4)$) and one-electron transitions ('1'=$3d_{3/2}4s_{1/2}(1) - 3d_{3/2}4d_{5/2}(4)$ and '2'=$3d_{3/2}4s_{1/2}(1) - 3d_{3/2}4d_{5/2}(3)$). The sharp features seen in the three other curves shown in the left central panel of Fig. 2 should be explained by change of the dominant contribution in the mixing coefficients considered in detail for the M1 transitions.

Transition rates for the six M2 lines from the $3d4s\ ^3D_3$ level are plotted in the left bottom panel of Fig. 2. We can see that three curves ('1', '3', and '4') are without any sharp feature, similar to three curves discussed above for the M3 transitions. All coupled states involved in those three transitions are easily identified by uncoupled states: $3d4s\ ^3D_3 \simeq 3d_{5/2}4s_{1/2}(3)$, $3d4p\ ^3D_1 \simeq 3d_{5/2}4p_{3/2}(1)$, $3d4p\ ^1F_3 \simeq 3d_{5/2}4p_{3/2}(3)$, and $3d4p\ ^3F_4 \simeq 3d_{5/2}4p_{3/2}(4)$. As a result, we find that those three transitions ('1', '3', and '4') are strongly one-electron transitions with large values of A_r without any sharp features. Sharp features in the curves labeled '5'=$3d4s\ ^3D_3 - 3d4f\ ^3P_2$ can be explained by a change of dominant contribution in mixing coefficients for the $3d4f\ ^3P_2$ level ($3d_{5/2}4f_{7/2}(2)$, $3p_{3/2}4s_{1/2}(2)$, and $3d_{3/2}4p_{3/2}(2)$) shown in Graph 2 of Ref. [11].

Four E3 transitions are illustrated in the right bottom panel of Fig. 2. The largest value of A_r is for the $3d4s\ ^3D_3 - 3d4f\ ^3D_1$ transition describing by curve '1'. Strong mixing between $3d_{5/2}4f_{7/2}(1)$ and $3p_{3/2}4s_{1/2}(1)$ states leads to the minimum in this curve for Z = 55–58. Even with those change of dominant state the $3d4s\ ^3D_3 - 3d4f\ ^3D_1$ transition is counted as a one-electron transition. Three other curves shown in the right bottom panel of Fig. 2 are two-electron transitions. Those transitions with small values of A_r are more sensitive to the change of dominant contribution than one-electron transitions. We can compare very deep minima on the curves '4' and '1'. The deep minimum in the curves '4'=$3d4s\ ^3D_3 - 3p4d\ ^3D_1$ at Z = 65 is due to strong mixing between the $3p_{3/2}4d_{3/2}(1)$ and $3s_{1/2}4p_{1/2}(1)$ states.

B. Wavelengths and transition rates

In Table IV, we present our RMBPT calculations for E2, M1, and M3 transition rates and wavelengths in the case of Ni-like tungsten, Z=74. For illustration, we choose transitions inside of the $3d4s$, $3d4p$, and $3d4d$ configurations. Wavelengths for those types of transitions for W^{46+} change from 120 Å up to 10400 Å. In Table IV, we also list the atomic properties for the $3d4s - 3d4d$, $3d4s - 3s4s$, and $3d4d - 3s4d$ transitions. Wavelengths for the $3d4s - 3d4d$ transitions are about 30–40 Å; however, the wavelengths of the $3d4s - 3s4s$ and $3d4d - 3s4d$ transitions are in a very narrow region, 12.4–12.5 Å for Ni-like tungsten. As can be seen from Table IV, the largest values of transition rates are for E2 transitions and the smallest are for M3 transitions. The value of A_r changes drastically (see Eq. (11)) with changes of wavelengths.

In Table V, we compare our RMBPT results for M1 and E2 transition rates with theoretical results presented by Biémont in Ref. [5]. We list results for transitions inside of $3d4s$ and $3d4p$ excited states in high-Z ions (Z= 92, 90, 83, and 80). As can be seen from Table V, the difference between both results is about 5 - 20% and can be explained by the second order contribution included in our RMBPT calculations, since the results in Refs. [5] were obtained in the MCDF approximation. We found surprisingly good agreement in wavelength (about 0.5%).

C. Lifetime data

The general trends of the Z-dependence of the lifetimes for the $3d4s\ ^{1,3}D_J$ levels in Ni-like ions are presented in Fig. 3. The Z-dependences of the lifetimes are smoother than the Z-dependence of the transition rates presented in Fig. 2. There are no sharp features in the curves shown in Fig. 3. The difference in the values of the lifetimes for the $3d4s\ ^3D_2$ and $3d4s\ ^1D_2$ levels is about 10–40%.

TABLE VII: Lifetime values (τ in sec.) of $3d4d\ ^{1,3}D_J$ levels of Ni-like ions.

	First-order RMBPT				Second-order RMBPT			
Z	$^3D_3$	$^3D_2$	$^3D_1$	$^1D_2$	$^3D_3$	$^3D_2$	$^3D_1$	$^1D_2$
42	2.90[+00]	1.16[-07]	3.83[-03]	8.16[-08]	3.14[+00]	1.69[-07]	3.89[-03]	1.19[-07]
47	2.18[-01]	2.07[-08]	5.18[-04]	1.89[-08]	2.30[-01]	2.68[-08]	5.33[-04]	2.43[-08]
50	6.24[-02]	9.19[-09]	1.81[-04]	9.27[-09]	6.59[-02]	1.08[-08]	1.90[-04]	1.17[-08]
54	1.49[-02]	3.68[-09]	5.15[-05]	4.08[-09]	1.55[-02]	4.42[-09]	5.33[-05]	4.86[-09]
55	1.08[-02]	2.99[-09]	3.82[-05]	3.38[-09]	1.12[-02]	3.56[-09]	3.64[-05]	4.04[-09]
56	7.86[-03]	2.46[-09]	2.87[-05]	2.82[-09]	8.19[-03]	2.91[-09]	2.88[-05]	3.38[-09]
60	2.48[-03]	1.19[-09]	9.74[-06]	1.45[-09]	2.57[-03]	1.38[-09]	9.76[-06]	1.65[-09]
70	2.37[-04]	2.75[-10]	9.37[-07]	3.61[-10]	2.43[-04]	3.08[-10]	9.37[-07]	3.98[-10]
74	1.08[-04]	1.69[-10]	4.12[-07]	2.26[-10]	1.11[-04]	1.88[-10]	4.12[-07]	2.47[-10]
79	4.47[-05]	9.79[-11]	1.59[-07]	1.32[-10]	4.57[-05]	1.08[-10]	1.58[-07]	1.43[-10]
80	3.79[-05]	8.84[-11]	1.32[-07]	1.19[-10]	3.87[-05]	9.72[-11]	1.32[-07]	1.29[-10]
83	2.36[-05]	6.59[-11]	7.76[-08]	8.90[-11]	2.40[-05]	7.21[-11]	7.76[-08]	9.56[-11]
90	8.73[-06]	3.56[-11]	2.45[-08]	4.78[-11]	8.87[-06]	3.88[-11]	2.44[-08]	5.10[-11]
92	6.75[-06]	3.04[-11]	1.79[-08]	4.06[-11]	6.85[-06]	3.30[-11]	1.78[-08]	4.31[-11]

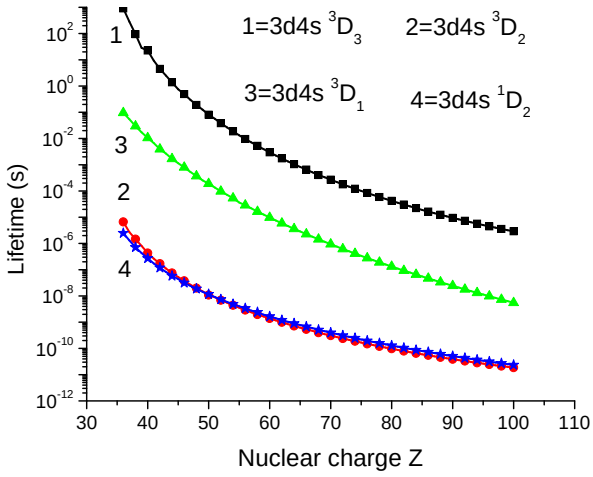

FIG. 3: Lifetimes of the even-parity states as a function of Z in sec.

TABLE VIII: Theoretical and experimental lifetimes (ms) of $3d4d\ ^3D_3$ level in Xe^{26+}, Cs^{27+}, and Ba^{28+} ions. Present theoretical result from the first-order RMBPT (a) and second-order RMBPT (b) are compared with other theoretical results from Refs. [1] (c), [8] (d) and experimental measurements from Refs. [1] (f) and [9] (g). All theoretical lifetimes are calculated in the absence of hyperfine structure (HFS).

		This work		Other	Experiment	
Z	Ion	(a)	(b)	theory	with HFS	no HFS
54	Xe^{26+}	14.9	15.5	14.0[c]	11.5± 0.5[f]	15.06±0.24[g]
54				15.12[d]		
55	Cs^{27+}	10.8	11.2		8.2± 2.0[f]	
56	Ba^{28+}	7.86	8.19		4.3± 3.6[f]	

Results of the present calculation of the lifetimes are obtained by taking into account multipole transition rates from each upper level to all possible lower levels. The contributions of the multipole transition rates to the lifetimes of the $3d4s\ ^{1,3}D_J$ levels with $J = 1$–3 are shown in Fig. 4.

The lifetime of the $3d4s\ ^3D_1$ level is defined by the sum of the five M1 and E2 transitions: $A^{M1}(3d^{10}\ ^1S_0 - 3d^94s\ ^3D_1)$, $A^{M1}(3d^94s\ ^3D_2 - 3d^94s\ ^3D_1)$, $A^{E2}(3d^94s\ ^3D_2 - 3d^94s\ ^3D_1)$, $A^{E2}(3d^94s\ ^3D_3 - 3d^94s\ ^3D_1)$, and $A^{E1}(3d^94p\ ^3F_2 - 3d^94s\ ^3D_1)$. The Z dependencies of these transition rates are shown in the top left panel of Fig. 4. As can be seen from this panel, the curve describing the $A^{E1}(3d^94p\ ^3F_2 - 3d^94s\ ^3D_1)$ transition rates starts from high-Z ($Z = 85$). This decay branch is enabled by the level inversion that occurs at the interface between the even- and odd-parity groups. In particular, even-parity levels cross various levels of the upper odd-parity group as Z increases (see for detail Ref. [28]). The contribution of this transition to the sum of all possible transitions is not very high, about 1% at $Z = 92$. The largest contribution in ΣA_r is given by the $A^{M1}(3d^94s\ ^3D_2 - 3d^94s\ ^3D_1)$ transition rate. The ratio of the $A^{M1}(3d^{10}\ ^1S_0 - 3d^94s\ ^3D_1)$ and $A^{M1}(3d^94s\ ^3D_2 - 3d^94s\ ^3D_1)$ transition rates is only about 0.01–0.02. This ratio is surprisingly small as both transitions are M1 decays, and the transition energy of the weaker decay is orders of magnitude larger. Tabulated data for the largest contribution in the lifetime the $3d4s\ ^3D_1$ level are listed in Table VI. In this table, we present the wavelengths and transition rates for the $3d4s\ ^3D_2 - 3d4s\ ^3D_1$ M1 transition. Tabulated data are given for Ni-like ions with $Z = 34$–100.

The opposite occurs for the $3d^94s\ ^3D_2$ and $3d^94s\ ^1D_2$ levels: the ratio of the $A^{E2}(3d^{10}\ ^1S_0 - 3d^94s\ ^3D_2)$ and $A^{E2}(3d^{10}\ ^1S_0 - 3d^94s\ ^1D_2)$ transitions rates to the sum of all multipole transition rates between the $3d^94s\ ^{1,3}D_J$

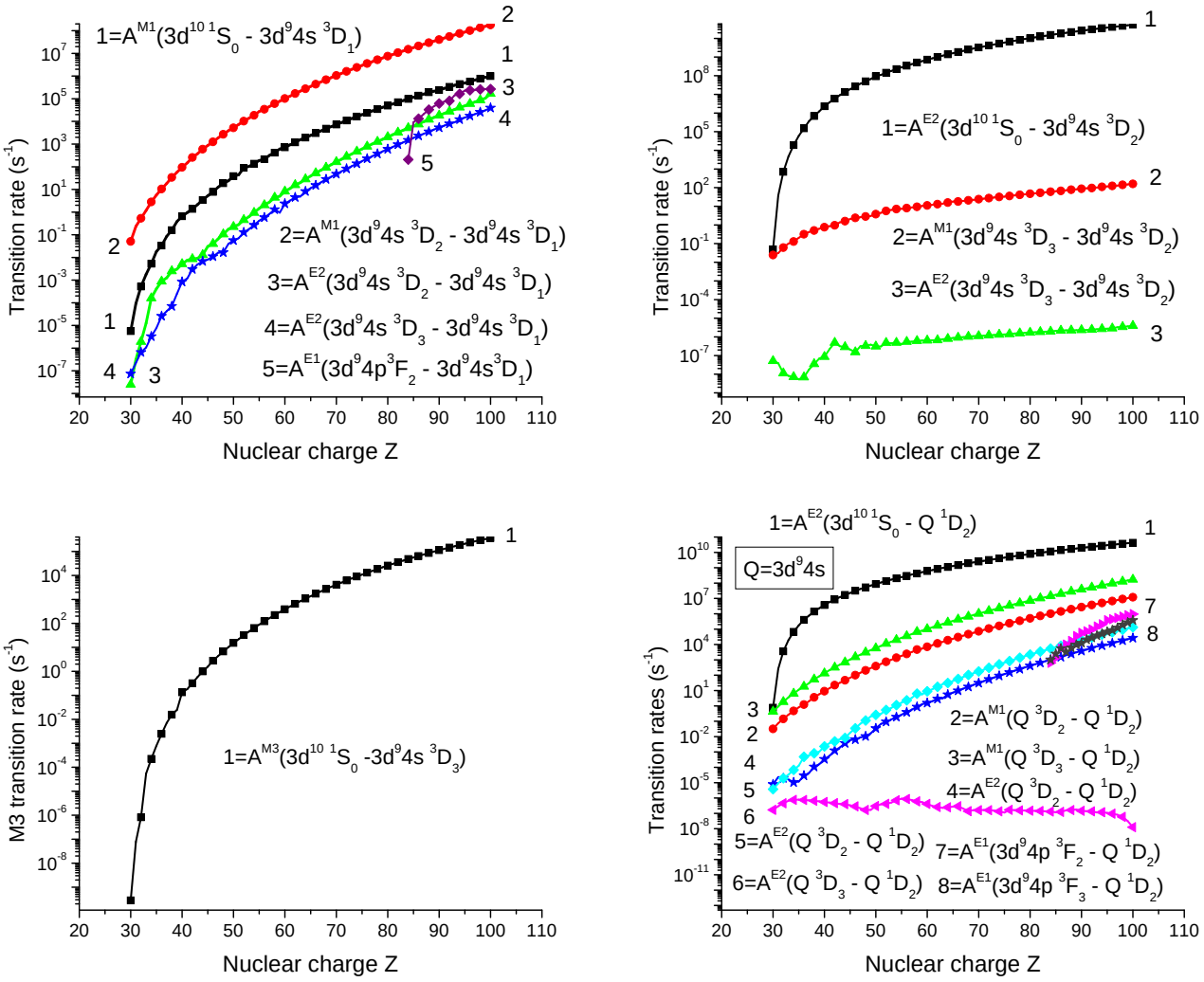

FIG. 4: Transition rates for $3d4s\ ^{1,3}D_J$ transitions in Ni-like ions as a function of Z.

excited states is equal to 10^7–10^8 and 10^4–10^5, respectively. Only the transition to the ground state $3d^{10}\ ^1S_0$ defines the lifetime of the $3d^9 4s\ ^3D_3$ level as can be seen from the bottom left panel of Fig. 4. It should be noted that the values of A_r shown in this figure are slightly different from those data presented in Refs. [2, 11].

The three curves shown in the right top panel of Fig. 4 illustrate the Z-dependencies of the $A^{E2}(3d^{10}\ ^1S_0 - 3d^9 4s\ ^3D_2)$, $A^{M1}(3d^9 4s\ ^3D_3 - 3d^9 4s\ ^3D_2)$, and $A^{E2}(3d^9 4s\ ^3D_3 - 3d^9 4s\ ^3D_2)$ transition rates. There is only the $3d^9 4s\ ^3D_3$ level below the $3d^9 4s\ ^3D_2$ level apart from the ground state $3d^{10}\ ^1S_0$. We already mentioned that the largest contribution to the lifetime of the $3d^9 4s\ ^3D_2$ level is given by the transition to the ground state. The smallest contribution is given by the $3d^9 4s\ ^3D_3 - 3d^9 4s\ ^3D_2$ E2 transition.

The even-parity complex with J=3 includes eleven states: $3d_{5/2}4s_{1/2}$, $3d_{5/2}4d_{3/2}$, $3d_{5/2}4d_{5/2}$, $3d_{3/2}4d_{3/2}$, $3d_{3/2}4d_{5/2}$, $3p_{3/2}4p_{3/2}$, $3p_{3/2}4f_{5/2}$, $3p_{1/2}4f_{5/2}$, $3p_{3/2}4f_{7/2}$, $3p_{1/2}4f_{7/2}$, and $3s_{1/2}4d_{5/2}$. All these states were included in the evaluation of the lifetime of the $3d^9 4s\ ^3D_3$ level [2, 11]. We decided to decrease number of states included in the even-parity complex with J=3, by omitting the last three states $3p_{3/2}4f_{7/2}$, $3p_{1/2}4f_{7/2}$, and $3s_{1/2}4d_{5/2}$. We found that for the $3d^9 4s\ ^3D_3$ level, the ratio of the first-order energy correction $E^{(1)}$ and the Dirac energy $E^{(0)}$ is rather large (about 0.1). The ratios of the second- and first-order matrix elements for the $3p_{3/2}4f_{7/2}$, $3p_{1/2}4f_{7/2}$, and $3s_{1/2}4d_{5/2}$ states are also about 0.1 for Ni-like xenon. The equation for coupled matrix elements (Eq. (8)) is appropriate for the case where the ratios of $E^{(1)}/E^{(0)}$ and the second- and first-order matrix elements $(Z_K^{(2)}/Z_K^{(1)})$ are small. As a result, we cannot include the above mentioned states in the evaluation of Eq. (8) for the coupled matrix elements. It should be noted that the octupole matrix elements with K=3 (see, Eq. (8)) are more sensitive to the expansion parameter being small

than the dipole matrix elements with K=1.

We found also that the ratios of $Z_K^{(2)}$ and $Z_K^{(1)}$ are about 1 in some cases for neutral Ni and Ni-like ions with Z = 31-33. This why we do not include numerical results for low-Z ions.

The largest number of transitions involved in determining the lifetime of a given $3d^9 4s\ ^{1,3}D_J$ level is associated with the $3d^9 4s\ ^1D_2$ level (the right bottom panel of Fig. 4). In this panel, we show six of the twelve possible transitions. The values of $A^{E2}(3d^9 4s\ ^3D_1 - 3d^9 4s\ ^1D_2)$ and $A^{M3}(3d^9 4s\ ^3D_J - 3d^9 4s\ ^1D_2)$ with J = 1–3 are smaller than the A_r values among the transitions illustrated in the right bottom panel of Fig. 4. We also do not show curves with the electric-dipole $3d^9 4p\ ^3F_2 - 3d^9 4s\ ^1D_2$ and $3d^9 4p\ ^3F_3 - 3d^9 4s\ ^1D_2$ transitions. The A_r values of these transitions are non-zero in the region of Z = 84–100. We already mentioned that the dominant contribution in the lifetime values of the $3d^9 4s\ ^1D_2$ level is from the $3d^{10}\ ^1S_0 - 3d^9 4s\ ^1D_2$ E2 transition. The contribution of all other transitions increases with Z; however, their contributions are only 0.1% for the W^{46+} ion.

In Table VII, we compare our results for the lifetimes of the $3d4s\ ^{1,3}D_J$ levels obtained in the first-order and second-order RMBPT approximations. Tabulated data are given for Ni-like ions with Z = 42–92. The smallest difference between the two approximations is for the $3d4s\ ^3D_1$ level (1–2%). There is also only a small difference between the two approximations for the $3d4s\ ^3D_3$ level when we truncate the basis set.

In Table VIII, theoretical and experimental lifetimes of the $3d4d\ ^3D_3$ level in the Xe^{26+}, Cs^{27+}, and Ba^{28+} ions are given. The present theoretical results evaluated in first- and second-order RMBPT are compared with other theoretical results from Refs. [1, 7, 8, 29, 30] and the measurements from Refs. [1, 9].

Both results (a) and (b) agree with the results for Cs^{27+} and Ba^{28+} given by Träbert *et al.* [1] when taking into account uncertainties given in [1]. Moreover, the measurements reported in [1] were for natural isotope mixture containing both odd and even isotopes. Odd isotopes have hyperfine structure and mixing as shown in [7, 8]. Our calculation do not include hyperfine structure and one should regard the comparison between our results and those in [1] with caution. However, a definitive comparison can be made with experimental result reported for $^{132}Xe^{26+}$ [9]. In this case, our values evaluated in a first- and second-order RMBPT approximation (see Table VIII) agree about equally well with the experimental result given by Träbert *et al.* [9]. The theoretical result given by Yao *et al.* [7, 8] is in the best agreement with the experimental result reported by Träbert *et al.* [1].

IV. CONCLUSION

We have presented a systematic second-order relativistic MBPT study of the reduced matrix elements, line strengths, and transition rates for electric-multipole and magnetic-multipole transitions between $3s^2 3p^6 3d^9 4l$, $3s^2 3p^5 3d^{10} 4l$, and $3s 3p^6 3d^{10} 4l$ states (with $4l$ = $4s$, $4p$, $4d$, and $4f$) in Ni-like ions with the nuclear charges ranging from Z = 34 to 100. Our retarded E2, E3, M1, M2, and M3 matrix elements include correlation corrections from Coulomb and Breit interactions. Both length and velocity forms of the E2 and E3 matrix elements were evaluated, and small differences, caused by the nonlocality of the starting DF potential, were found between the two forms. Contributions from negative energy states were also included in order to improve the agreement between results calculated in lengths and velocity gauges. Second-order RMBPT transition energies were used in our evaluation of the line strengths, transition rates, and lifetimes. These calculations are compared with other calculations and with available experimental data. The relativistic atomic data calculated in this paper can motivate future experiments with long-lived excited levels of heavy ions. In particular it can lead to better understanding of atomic structure and high-multiple order decay processes in electron beam ion trap and laboratory plasmas experiments

Acknowledgments

This research was sponsored by the National Nuclear Security Administration under Cooperative agreement DE-FC52-06NA27588 and in part by the grant DE-FG02-08ER54951. Work at LLNL was performed under auspices of the DOE under contract No. DE-AC52-07NA2344. We thank E. Träbert for helpful comments on the manuscript. Prepared by LLNL under Contract DE-AC52- 07NA27344.

[1] E. Träbert, P. Beiersdorfer, G. V. Brown, K. Boyce, R. L. Kelley, C. A. Kilborne, F. S. Porter, and A. Szymkowiak, Phys. Rev. A **73**, 22508 (2006).
[2] E. Träbert, P. Beiersdorfer, G. V. Brown, S. Terracol, and U. I. Safronova, Nucl. Instr. Methods Phys. Res. B **235**, 23 (2005).
[3] Yu. Ralchenko, J. N. Tan, J. D. Gillaspy, J. M. Pomeroy, and E. Silver, Phys. Rev. A **74**, 042514 (2006).
[4] P. Beiersdorfer, A. L. Osterheld, J. Scofield, B. Wargelin, and R. E. Marrs, Phys. Rev. Lett. **67**, 2272 (1991).
[5] E. Biémont, J. Phys. B **39**, 4207 (1997).
[6] E. Biémont, Phys. Scr. T **73**, 59 (1997).
[7] K. Yao, M. Andersson, T. Brage, R. Hutton, P. Jönsson, and Y. Zou, Phys. Rev. Lett. **97**, 183001 (2006).
[8] K. Yao, M. Andersson, T. Brage, R. Hutton, P. Jönsson, and Y. Zou, Phys. Rev. Lett. **98**, 269903 (2007).

[9] E. Träbert, P. Beiersdorfer, and G. V. Brown, Phys. Rev. Lett. **98**, 263001 (2007).
[10] S. M. Hamasha, A. S. Shlyaptseva, and U. I. Safronova, Can. J. Phys. **82**, 331 (2004).
[11] U. Safronova, A. S. Safronova, S. M. Hamasha, and P. Beiersdorfer, At. Data Nucl. Data Tabl. **92**, 47 (2006).
[12] U. I. Safronova, A. S. Safronova, and P. Beiersdorfer, J. Phys. B **39**, 4491 (2006).
[13] R. Neu, K. B. Fournier, D. Schlögl, and J. Rice, J. Phys. B **30**, 5057 (1997).
[14] K. Asmussen, K. B. Fournier, J. M. Laming, R. Neu, J. F. Seely, R. Dux, and W. Engelhardt, Nuclear Fusion **38**, 917 (1998).
[15] S. R. Elliott, P. Beiersdorfer, B. J. MacGowan, and J. Nilsen, Phys. Rev. A **52**, 2689 (1995).
[16] P. G. Burkhalter, C. M. Dozier, and D. J. Nagel, Phys. Rev. A **15**, 700 (1977).
[17] A. Shlyaptseva, D. Fedin, S.Hamasha, C. Harris, V. Kantsyrev, P. Neill, N. Quart, U. I. Safronova, P. Beiersdorfer, K. Boyce, et al., Rev. Scientific Instr. B **75**, 3750 (2004).
[18] A. S. Safronova, V. L. Kantsyrev, D. A. Fedin, G. Osborne, M. F. Yilmaz, T. Hoppe, V. Nalajala, J. D. Douglass, R. D. McBride, M. D. Mitchell, et al., IEEE Transactions Plasma Science **34**, 2256 (2006).
[19] P. Neill, C. Harris, A. S. Safronova, S. M. Hamasha, S. Hansen, U. Safronova, and P. Beiersdorfer, Can. J. Phys. **82**, 931 (2004).
[20] R. Hutton, Y. Zou, J. Reyna Almandos, C. Biedermann, R. Radtke, A. Greier, and R. Neu, Nucl. Instr. Methods Phys. Res. B **205**, 114 (2003).
[21] R. Radtke, C. Biedermann, J. L. Schwob, P. Mandelbaum, and R. Doron, Phys. Rev. A **64**, 12720 (2001).
[22] W. R. Johnson, D. R. Plante, and J. Sapirstein, Advances in Atomic, Molecular, and Optical Physics **35**, 255 (1995).
[23] U. I. Safronova, W. R. Johnson, and J. R. Albritton, Phys. Rev. A **62**, 052505 (2000).
[24] M. H. Chen, K. T. Cheng, and W. R. Johnson, Phys. Rev. A **47**, 3692 (1993).
[25] U. I. Safronova, W. R. Johnson, D. Kato, and S. Ohtani, Phys. Rev. A **63**, 032518 (2001).
[26] U. I. Safronova, W. R. Johnson, and A. Derevianko, Phys. Scr. **60**, 46 (1999).
[27] U. I. Safronova, Mol. Phys. **98**, 1213 (2000).
[28] U. I. Safronova, A. S. Safronova, and P. Beiersdorfer, J. Phys. B **40**, 955 (2007).
[29] T. G. Walker and C. J. Goebel, Phys. Rev. Lett. **98**, 269303 (2007).
[30] K. Yao, M. Andersson, T. Brage, R. Hutton, P. Jönsson, and Y. Zou, Phys. Rev. Lett. **98**, 269304 (2007).